Unbinding of Translocator Protein 18 kDa (TSPO) ligands: from in vitro residence time to in vivo efficacy via in silico simulations.

Agostino Bruno[†], Elisabetta Barresi[‖], Nicola Simola[‡], Eleonora Da Pozzo[‖], Barbara Costa[‖], Ettore Novellino[†], Federico Da Settimo[‖], Claudia Martini[‖], Sabrina Taliani[‖]*, and Sandro Cosconati[§]*.

[†]*Department of Pharmacy, University Federico II of Naples, Via D. Montesano 49, 80131 Naples, Italy.*

[‖]*Department of Pharmacy, Università di Pisa, Via Bonanno 6, 56126 Pisa, Italy.*

[‡]*Department of Biomedical Sciences, University of Cagliari, Monserrato University Campus, 09042 Monserrato, Italy.*

[§]*DiSTABiF, University of Campania "Luigi Vanvitelli", Via Vivaldi 43, 81100 Caserta, Italy*.

Abstract. The Translocator Protein 18 kDa (TSPO) is a validated pharmacological target for the development of new treatments for neurological disorders. *N,N*-Dialkyl-2-phenylindol-3-ylglyoxylamides (PIGAs) are effective TSPO modulators and potentially useful therapeutics for the treatment of anxiety, CNS pathologies featuring astrocyte loss, and inflammatory-based neuropathologies. For this class of compounds, no correlation exists between the TSPO binding affinity and the corresponding functional efficacy. Rather, their biological effectiveness correlates with the

kinetics of the unbinding events and more specifically with the residence time (RT). So far, the structural reasons for the different recorded RT of congeneric PIGAs remain elusive. Here, to understand the different kinetics of PIGAs, their unbinding paths were studied employing enhanced-sampling molecular dynamics simulations. Results of these studies revealed how subtle structural differences between PIGAs have a substantial effect on the unbinding energetics. In particular, during the egress from the TSPO binding site, slow-dissociating PIGAs find tight interactions with the protein LP1 region thereby determining a long RT. Further support to these findings was achieved by in vivo studies demonstrating how the anxiolytic effect observed for the inspected PIGAs correlates with their RT to TSPO.

Keywords: Translocator Protein 18 kDa, Neuroactive Steroids, Residence Time, Molecular Dynamics, Unbinding Event, Potential of Mean Force.

Introduction

Thermodynamic binding affinity has been long used as the major predictor of in vivo drug potency, and thus applied as a basis for lead optimization step of the drug discovery pipeline. More recently, a number of studies highlighted that the affinity displayed by ligand for its target *per se* might not directly describe its biological efficacy, and that kinetics could represent a key parameter to consider during lead optimization and preclinical development.[1,2]

Thus, much attention has been posed toward the determination of the ligand association and dissociation rate constants (k_{on} and k_{off}, respectively) to describe the persistence of the binary drug–target complex. Of particular interest is the kinetics of the unbinding event, often referred to as residence time (RT = $1/k_{off}$), because the slow drug–target dissociation rate seems to be the main critical molecular determinant for pharmacological activity.[1,2] Actually, it has been shown that a long RT can better translate into in vitro/in vivo efficacy than affinity itself.[1] In this scenario, RT is now considered as a key parameter in drug

discovery programs for a number of ligand-target systems including ligands for several G protein-coupled receptors (GPCR), HIV protease inhibitors, kinase inhibitors, and so on.[1]

Our research group has been actively involved in the discovery of chemical modulators of the Translocator Protein 18 kDa (TSPO) for which we described a specific class, the *N,N*-dialkyl-2-phenylindol-3-ylglyoxylamides (PIGAs).[3-5] TSPO is an outer mitochondrial membrane protein[6] expressed at high levels in peripheral and central nervous system (CNS) steroid-producing cells.[6,7] It is recognized as a major target to promote the biosynthesis of neuroactive steroids, which exert potent antidepressant, anxiolytic, sedative, anticonvulsant, amnesic and analgesic effects, mostly acting by positively modulating the γ-aminobutyric acid type A receptor (GABA$_A$R) in an allosteric manner.[7,8] Furthermore, these neuroactive molecules exert neurotrophic, neuroprotective, anti-apoptotic and anti-inflammatory activities in several animal models of cerebral ischemia, traumatic brain and spinal cord injury, peripheral neuropathy, and neurodegenerative pathologies.[8] In particular, TSPO plays a pivotal function in the transportation of the cholesterol into mitochondria that represents the rate-limiting step of the synthesis of neuroactive steroids; once in the mitochondria, cholesterol is converted by the cytochrome P450 enzyme CYP11A1 into pregnenolone, which is the precursor of all neurosteroids.[7,8]

Several TSPO ligands, including PIGAs, are able to strongly and dose-dependently induce steroid biosynthesis in steroidogenic cells, and they have been suggested to be potential novel therapeutics in several CNS pathologies.[9-13] Actually, a number of our PIGAs promote the protection of human astrocytes and prevent oxidative damage as well as inflammation in an in vitro neuroinflammatory model.[14,15] These studies suggested that PIGAs could represent potential novel therapeutics for CNS diseases featuring dysregulated activation of astrocyte functions and/or for inflammatory-based neuropathologies.[15] Furthermore, some PIGAs have been evaluated in vivo by means of the elevated plus-maze (EPM) test in

rats, showing promising anxiolytic-like properties.[4,11,16] In all cases, the observed effects were related to a stimulation of endogenous neurosteroid production.[14-16]

In this respect, we also recently reported the results of radioligand kinetic studies[17,18] on a number of our previously described PIGAs, that address one of the most critical issues concerning TSPO ligands, namely the poor correlation between binding affinity and steroidogenic efficacy. This has hampered the identification of efficacious lead compounds by traditional affinity-based drug discovery strategies and often questions the specificity of the biological effects.[19] Studies conducted on a set of PIGAs, selected in virtue of their different capabilities of inducing in vitro steroidogenesis despite the very similar TSPO binding affinity, indicated that RT is the main parameter to consider for robust neurosteroidogenic ligand efficacy.[17,18] Along this line, the determination of this kinetic parameter during the in vitro characterization of a TSPO ligand is required to obtain structure–efficacy relationships suitable to develop new compounds with favorable pharmacological features. However, binding and unbinding kinetics determination of TSPO ligands requires expensive setup and time-consuming testing of several newly synthesized compounds in rather complex and expensive radioligand kinetic assays.[17]

All these findings ask for an enhanced perception of the structure−kinetic relationship (SKR) of our PIGAs. A major complication when profiling SKRs resides in the characterization at molecular level of the different metastable binding conformations that the ligand experiences when associating to and dissociating from the target structure. These metastable states ultimately influence the final RT values of a ligand. The application of in silico methods can offer the invaluable opportunity to deliver, in a cost-effective way, an estimation of RT of a ligand, as well as capturing the dynamic processes implicated in compound dissociation that currently available assays cannot afford. In particular, molecular dynamics (MD) simulations are valuable methods to gain insights into the dissociation of a ligand from the binding cavity of the cognate biological target. Nevertheless, unbinding events usually occur in very long time

scales (milliseconds) which can be hardly sampled in standard MD calculations. In this respect, enhanced sampling methods like steered MD (SMD)[20] random acceleration MD (RAMD),[21] and metadynamics[22] have been extensively used to unravel the unbinding kinetics of ligand-target complexes. Among these methods, in SMD the ligand is forced to dissociate from the biological target through the application of a guiding potential along a defined reaction coordinate with a constant force or a constant velocity applied to the studied ligand. Moreover, analysis of the SMD trajectories, employing the Jarzynski's equality,[23] allows for the determination of the potential of mean force (PMF) and the ΔF_{off} which is related to the dissociation rate constants (k_{off}). RAMD is an additional enhanced-sampling method in which a random force, imposed to the ligand's center of mass, permits the studied binder to explore a wider conformational space.

In this work, we employed SMD in tandem with RAMD calculations to study the unbinding of TSPO PIGA ligands (**1** and **2** in Table 1) as well as the stereotypical TSPO ligand PK11195 (**3**). Results from these studies underscore that subtle structural modifications of our PIGA compounds have a substantial effect on the unbinding path and energetics of TSPO ligands. These data were supported by binding and functional in vitro studies as well as in vivo experiments. This work explains for the first time the molecular bases of the functional activity of TSPO ligands thereby providing the foundations for the design of new efficacious small molecules for this neuropharmacologically relevant target.

Results and Discussion

Two high-affinity TSPO ligands, **1** (K_i 0.91 nM) and **2** (K_i 0.34 nM), Table 1, were selected from our in-house PIGA database (Table S1, Supporting Information (SI))[3-5] considering their different kinetic parameters and efficiency in stimulating in vitro steroidogenesis.[17] Specifically, **1** and **2** (Table 1) represent prototypes of rapid (**1**, RT 17 min) and slow (**2**, RT 141 min) dissociating competitor of the [^{3}H]PK11195

binding site, respectively. In virtue of the significant positive correlation between the kinetic parameter RT and the efficacy to stimulate in vitro neurosteroidogenesis,[17] the two selected PIGAs show different neurosteroidogenic activity (Table 1) and, consequently, diverse pharmacological perspectives.

Table 1. Experimental kinetic/thermodynamic data and neurosteroidogenic efficacy for TSPO ligands.

Compd.	Equilibrium K_i (nM)[a]	K_{on} (M^{-1} . min^{-1})[a]	K_{off} (min^{-1})[a]	RT (min)[a]	Emax at 100 μM (vehicle set to 100%)[a,b]
1	0.91 ± 0.11	$5.78 \pm 0.5 \times 10^7$	0.058 ± 0.005	17 ± 1	149 ± 4
2	0.34 ± 0.03	$4.30 \pm 0.3 \times 10^7$	0.007 ± 0.001	141 ± 4	275 ± 5
3	3.39 ± 0.34	$9.30 \pm 0.9 \times 10^6$	0.029 ± 0.003	34 ± 3	153 ± 4

[a]Data taken from ref. 17. [b]Efficacy (Emax) corresponds to the amount of pregnenolone production induced by 100 μM TSPO ligand concentration.

Taking advantage of the rat (r) TSPO three-dimensional (3D) model previously developed by us,[5] in this study, docking calculations were performed for **1** and **2**. As stated above, these ligands feature comparable potencies in displacing [^{3}H]PK11195, but different k_{off} values and, consequently, different RTs, with **2** having a lower k_{off} and longer RT with respect to those of **1** (Table 1). Moreover, in this inspection, we also considered **3** as a control compound. Analysis of the theoretical binding poses achieved for **2** (Figure 1B) confirmed the results already achieved for a structural congener.[5] Briefly, the indole ring is embedded in a hydrophobic cleft formed by A23, W53, L49, and W143 while the 2-naphthyl moiety is placed inside an aromatic cleft establishing hydrophobic interactions with V110, W95, W107, L114, W143, F146, and L150 residues. Moreover, the *N-n*-pentyl branch extends toward the external portion of the receptor taking

contacts with L31 and H43 that belong to the TM1-TM2 loop (LP1). In general, the same interaction pattern was also calculated for **1** (Figure 1A) although the different substituents at the glyoxylamide nitrogen atom (two *N-n*-butyl chains) allow the ligand to establish additional interactions with L49 residue. The binding mode of **3** (Figure 1C) is not described here as it is virtually superimposable to the experimental one achieved through NMR studies attained on the mouse (m) TSPO.[24]
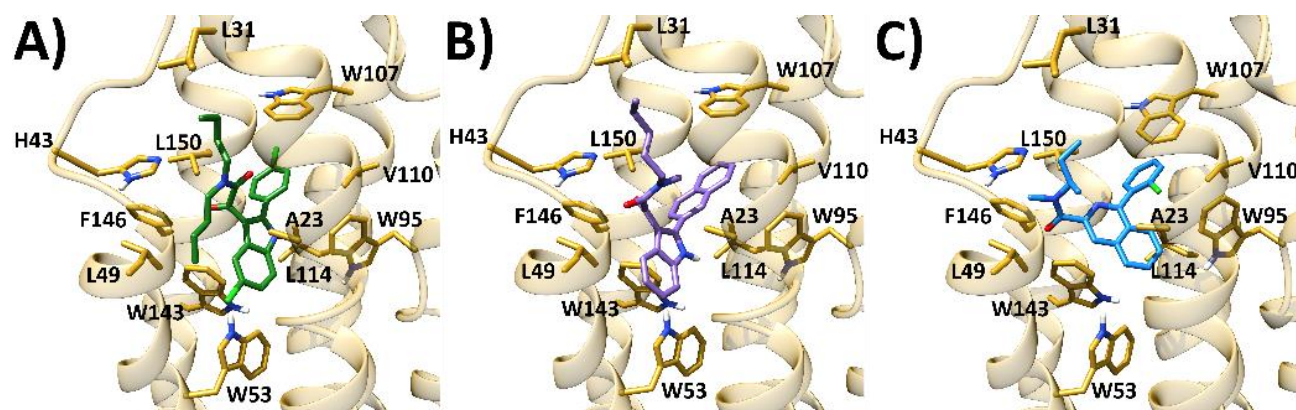
Figure 1. Binding mode of **1** (A), **2** (B), and **3** (C) into the rTSPO model. **1**, **2**, and **3** are depicted as green, violet and blue sticks, respectively. The protein is represented as yellow sticks and ribbons.

MD simulations have proven to be effective tools in elucidating the structural features determining kinetic aspects of unbinding processes of relevant protein-ligand complexes.[25-30] In particular, SMD simulations approaches have been applied as a powerful and flexible method to provide information about energetic and structural features driving protein-ligand unbinding events, and details on time-resolved complex dissociation.[29-31] In this work, by employing SMD simulations (see methods), we aimed at providing detailed profiling of the unbinding process of **1**, **2** and **3** from the TSPO ligand binding site. To estimate the free energy changes along the ligand unbinding, we reconstructed the PMF profiles of the three studied ligands dissociating from the rTSPO receptor. This was obtained by applying Jarzynski's equality (eq. 3

in molecular modeling methods) and the cumulative expansion up to the second order (eq. 4 in molecular modeling methods). This plot (Figure 2) reveals that the PMF of **2** ($\Delta F_{off}^2 = 86.65 \pm 4.57$ kcal/mol) is higher than that of **1** ($\Delta F_{off}^1 = 74.18 \pm 2.63$ kcal/mol), while the difference between **1** and **3** ($\Delta F_{off}^3 = 77.21 \pm 1.98$ kcal/mol) falls within the twilight zone of statistical significance, according to their standard deviations. Hence, according to these studies, **1** and **3** would more easily dissociate from the rTSPO than **2**. This agrees with the experimental k_{off} and RT values recorded for the three compounds (Table 1).
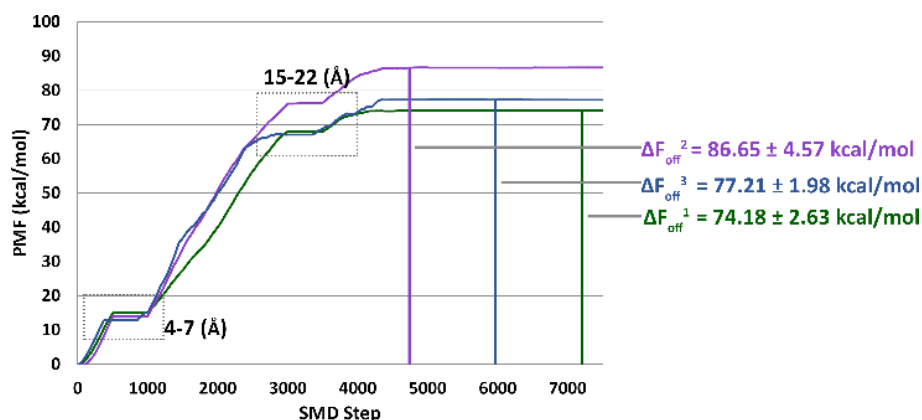

Figure 2. PMF plots achieved through SMD simulations for **1-3.**

Analysis of Figure 2 also reveals the presence of two main PMF shoulders, which occur where the ligand is at a 4-7 Å and 15-22 Å distance from the binding site, respectively. In particular, for the three studied ligands, the PMF increases sharply and to the same extent up to the first 4-7 Å displacement. On the other hand, in the second shoulder (at 15-22 Å from the binding site), **1** and **3** PMF profiles increase gradually while a different trend was observed for that of **2** indicating the presence of much tighter interactions with the receptor counterpart.

To get structural insight supporting the different behavior of the three ligands, we performed a cluster analysis in order to obtain a reduced number of representative structures describing the unbinding mechanism of all the ligands. This inspection outlined that in the first PMF shoulder (at 4-7 Å from the

primary binding site) the three ligands occupy the same cleft at the crevice between rTSPO helices TM2 and TM5 where the roof is made up by the LP1 loop (Figure 3A, B, and C).
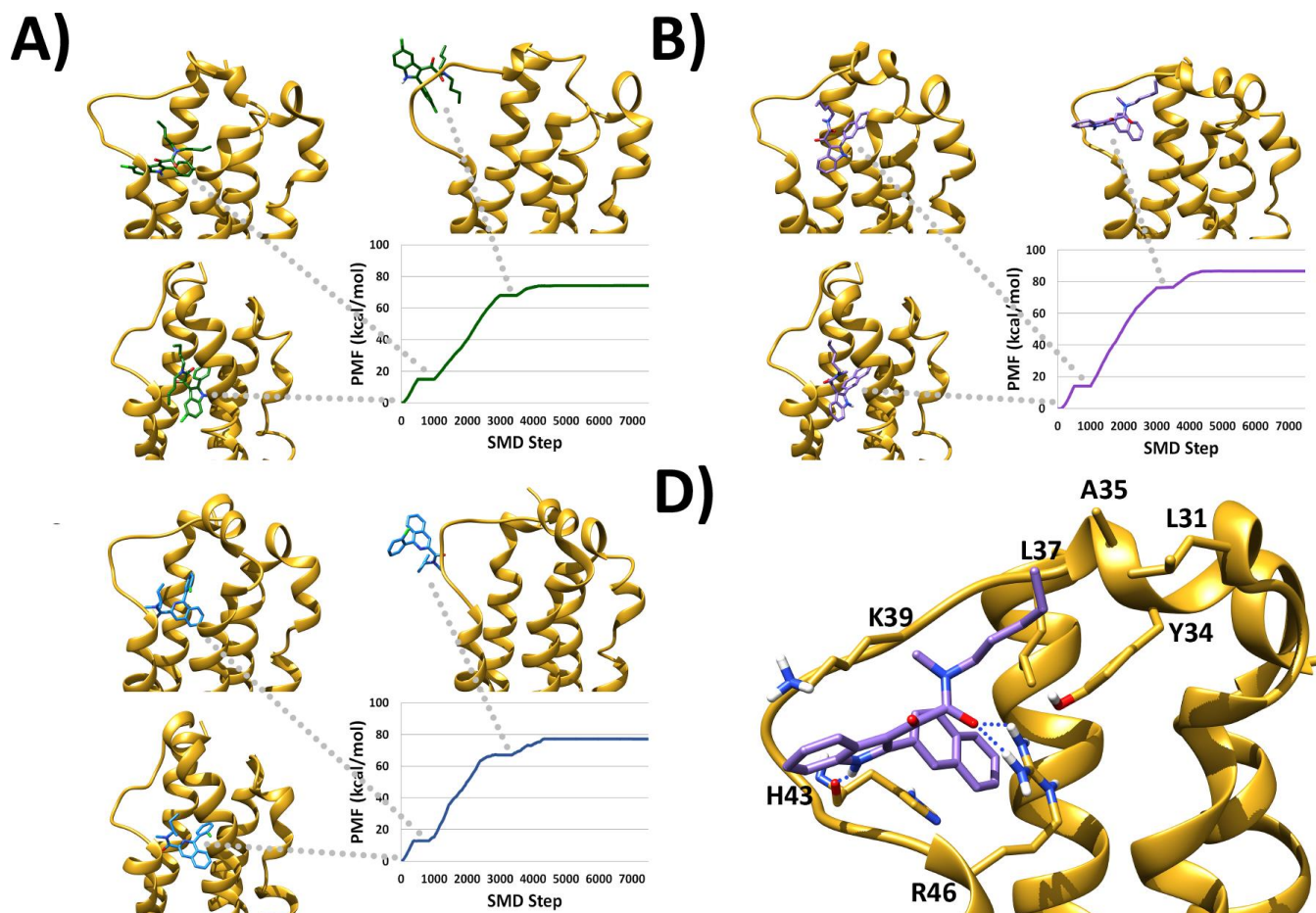
Figure 3. Binding modes into the rTSPO model adopted during the SMD simulations by the inspected ligands at the starting position, and at 4-7 Å and 15-22 Å distance from the binding site. **1** (A), **2** (B), and **3** (C) are depicted as green, violet, and blue sticks, respectively. The protein is represented as yellow sticks and ribbons. Panel D represents a close-up view of the binding pose adopted by **2** when at 15-22 Å distance from the binding site. H-bonds are represented by dashed blue lines.

Within this site, the three compounds take contact with the same set of residues, while the receptor structure adopts a similar overall folding in the three calculated complexes. This should explain why the three ligands do have the same PMF profile in this receptor region.

Conversely, when the ligands egress from this first meta-site and reach the second one (at 15-22 Å from the primary site), before finally leaving the rTSPO receptor, different interactions were recorded. Most specifically, in this receptor region, **1** and **3** make contact with the long LP1 loop that, in the meanwhile, has opened towards the cytosol thereby allowing the ligand to finally dissociate from its cognate protein (Figure 3A and C). On the contrary, at this stage, **2** is able to engage in tight interactions with the protein (Figure 3B and D). In particular, the indole aromatic core structure is pointing outwards forming an H-bond with the backbone CO of H43 belonging to the LP1 loop and a cation-π interaction with K39 side chain. Additionally, the pendant 2-naphthyl substituent is sandwiched between H43 of the aforementioned loop and R46 of TM2 forming tight π-π and cation-π interactions, respectively. The pose adopted by **2** also allows the glyoxylamide *N-n*-pentyl chain at position 3 of the indole core structure to take positive contacts with a solvent-exposed pocket of the LP1 loop formed by Y34, L31, A35 and L37 sidechains, while a further anchoring point is provided by the presence of a charge-reinforced H-bond between one of its carbonyl oxygens and R46 sidechain.

The involvement of this protein region in the formation of a meta-stable binding site, before all the ligands leave the target, is in accordance with results of site-directed mutagenesis experiments attained in several species outlining the role of the LP1 loop for ligand binding.[32,33] In particular, according to our studies, rather than directly influencing the binding affinity of the different ligands, we suggest that this loop is modulating the kinetic aspects of the unbinding process. Most precisely, the presence of tight interactions with the LP1 loop, during the egress of a TSPO ligand from the receptor binding site, will result in lower k_{off} values and longer RT. Consistently, in our simulations, **1** and **3** were not able to strongly interact with

the LP1 loop and this should explain why the three ligands, although having a comparable K_i at TSPO, do display different k_{off} and RT values. Here, we are also indicating that the reason for a lower k_{off} value recorded for **2** should be ascribed to the presence of the 2-naphthyl group that influences both the flexibility of the ligand and the interactions with the loop. This is also consistent with experimental data outlining a long RT also for another naphthyl-substituted PIGA (compound **11** in Table S1 of SI).[17]

To gain major insights into the unbinding event of the three studied ligands we also analyzed the unbinding pathway as a probability distribution in function of two different collective variables (CVs) (Figure 4): (*i*) the distance between the two centers of mass calculated for the ligand and the binding site residues (COMs) (CV1); (*ii*) the distance between P41 and T149, which describe the degree of opening of the LP1 loop with which the ligands interact during their egress from the protein (CV2). In Figure 4 it can be appreciated that, when dissociating from rTSPO, the three ligands induce difference degree of opening of the loop, where **2** is the one showing the greater variability, while **1** and **3** show similar behaviors. Moreover, for **1** and **2** it was possible to clearly identify one preferential unbinding route, where **2** requires a less opened loop with respect to **1**. On the contrary, for **3** two equally probable pathways were identified. To visualize the aforementioned unbinding pathways, we calculated the spatial occupancy maps of **2** (Figure 4D) and **1** (Figure 4E) over the SMD simulations. From this analysis, it is clear that **1** should leave the binding site from a lateral exit at the crevice formed by helices TM1 and TM5; conversely, **2** reaches the cytosol from the gate at the interface of TM1 and TM2 helices. Interestingly, in 2016 Li and colleagues[34] suggested that this TSPO region should constitute the lateral entrance to the protein binding cavity of hydrophobic ligands. In this work, we further refine this hypothesis by suggesting that, rather than the entrance, helices TM1, TM2, and TM5, as well as LP1, would mainly affect the exit of hydrophobic TSPO ligands from the receptor binding cavity.
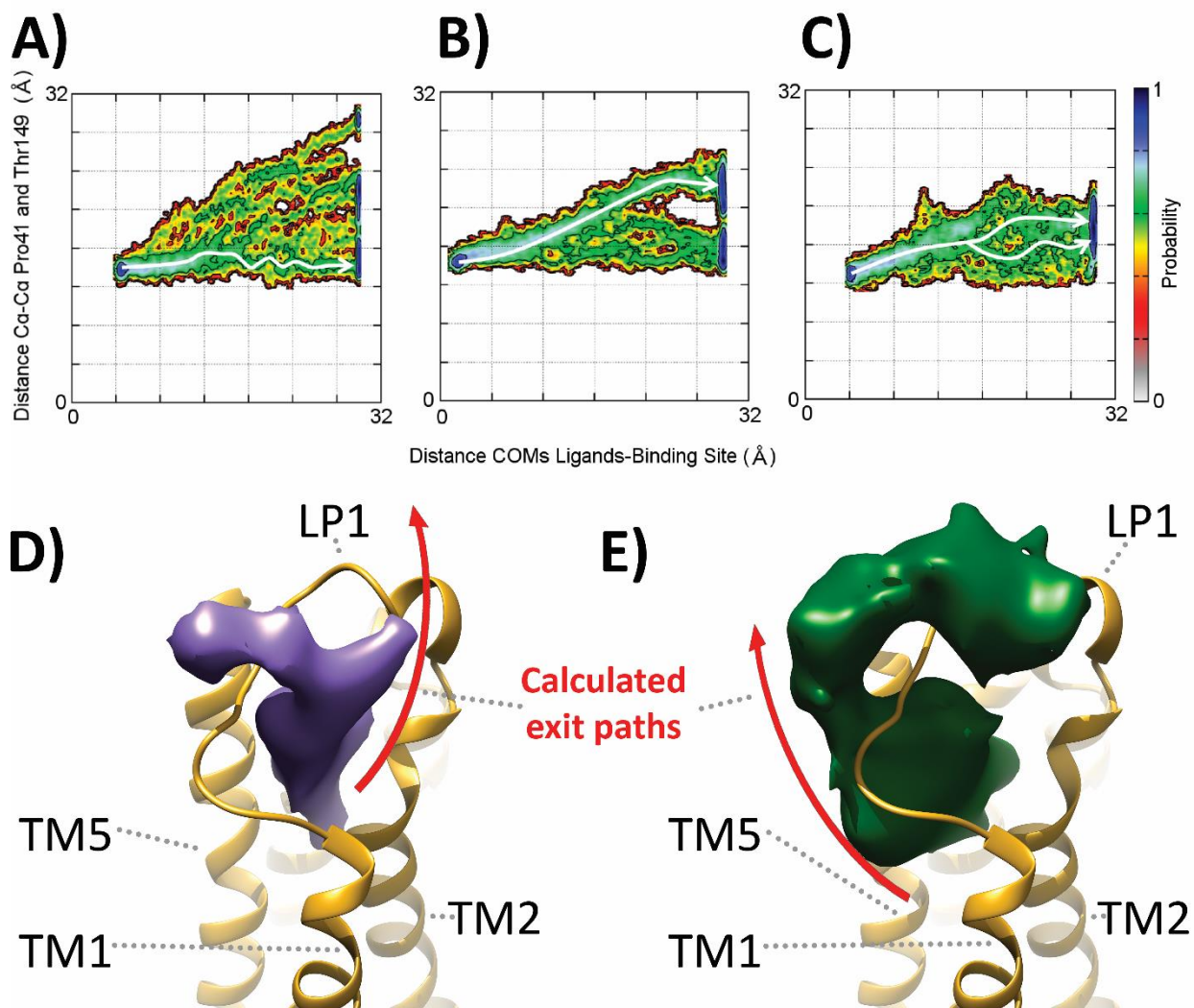
Figure 4. Probability distribution of **2** (A), **1** (B), and **3** (C) unbinding from rTSPO in function of CV1 and CV2. Spatial occupancy maps of **2** (D) and **1** (E): atoms are represented as violet and green surfaces in panels D) and E), respectively. The rTSPO structure is represented ad yellow ribbons.

All in all, our data suggest that the egress of the PIGA compounds from TSPO is mainly affected by the strength of interactions established by the ligand with LP1. This loop is in close proximity to the cholesterol recognition amino acid consensus (CRAC) motif.[32] Recent experiments by Zweckstetter and colleagues[35] demonstrated a direct interplay between the TSPO cholesterol binding and the protein oligomerization state. In particular, cholesterol binding to TSPO enhances the division of the mammalian

TSPO dimer into a monomer. This is because cholesterol binding to CRAC induces a long-range structural reorientation of the transmembrane bundle that is mediated by TM2 and ultimately sensed by the GxxxG dimerization motif in TM3. Our studies indicate that slow-dissociating PIGAs, by inducing a specific conformation of LP1 during their egress from the protein should influence the CRAC binding to cholesterol thereby acting as allosteric modulators of the oligomerization state of TSPO.

To further support our theoretical and biochemical studies, we next asked whether in vitro efficacies of the inspected PIGAs could translate into a difference in pharmacological effect in vivo. In this respect, the drug-like character of our compounds was first in silico evaluated by employing the Qikprop program (Schrödinger. LLC New York). A number of physicochemical and pharmacokinetic properties of **1** and **2** were calculated as a rough estimate of their potential to be CNS active (Table 2). Quantitative structure-activity relationship (QSAR) analyses, considering ligands active on CNS and related analogs along with studies on CNS active drugs, have proposed a set of physicochemical features that CNS ligands should have. They are molecular weight less than 450, number of H-bond acceptors less than 7, a polar surface area less than 90 Å, ClogP less than 5, and a number of rotatable bonds equal to or less than 10. Based on these properties, our PIGAs should have a high potential of reaching the CNS (Table 2), since all the calculated parameters are within the above-mentioned ranges. Furthermore, the QPPMDCK parameter, which estimates the penetration of MDCK cells (models of the blood-brain barrier (BBB)), indicates that **1** and **2** should have high brain penetration properties, with **1** having the highest BBB crossing probability

Table 2. Calculated physicochemical and pharmacokinetic properties of PIGAs **1** and **2**.

Compound	1	2	Range or recommended values[a]	Recommended values for CNS active drugs
#rotor[b]	8	6	0 – 15	≤10
#rtvFG[c]	2	2	0 – 2	
CNS[d]	0	0	–2 (inactive), +2 (active)	
mol_MW[e]	445.388	398.504	130.0 – 725.0	< 450
dipole[f]	5.828	4.715	1.0 – 12.5	
SASA[g]	709.989	706.449	300.0–1000.0	
donorHB[h]	0	0	0.0 – 6.0	
accptHB[i]	4	4	2.0 – 20.0	< 7
QPlogPo/w[j]	6.296	5.873	-2.0 – 6.5	< 5
QPlogS[k]	-6.817	-6.533	–6.5 – 0.5	
QPPCaco[l]	2899.12	3245.137	<25 poor, >500 great	
QPlogBB[m]	-0.174	-0.316	-3.0 – 1.2	
QPPMDCK[n]	7509.884	1765.763	<25 poor, >500 great	
Human Oral Absorption[p]	100	100	<25% poor, >80% high	

[a]For 95% of known drugs. [b]Number of non-trivial (not CX3), non-hindered (not alkene, amide, small ring) rotatable bonds. [c]Number of reactive functional groups. [d]Predicted central nervous system activity on a – 2 (inactive) to +2 (active) scale. [e]Molecular weight of the molecule. [f]Computed dipole moment of the molecule. [g]Total solvent accessible surface area (SASA) in square angstroms using a probe with a 1.4 Å radius. [h]Estimated number of hydrogen bonds that would be donated by the solute to water molecules in an aqueous solution. [i]Estimated number of hydrogen bonds that would be accepted by the solute from water molecules in an aqueous solution. [j]Predicted octanol/water partition coefficient. [k]Predicted aqueous solubility, log S. S in mol dm^{-3} is the concentration of the solute in a saturated solution that is in equilibrium with the crystalline solid. [l]Predicted apparent Caco-2 cell permeability in nm/sec. Caco-2 cells are a model for the gut-blood barrier. [m]Predicted brain/blood partition coefficient. [n]Predicted apparent MDCK cell permeability in nm/sec. MDCK cells are considered to be a good mimic for the blood-brain barrier. [o]Number of likely metabolic reactions. [p]Predicted qualitative human oral absorption.

Behavioral effects of **1** and **2** were assessed by evaluating rats' performance in the EPM, a test widely utilized to evidence anxiety-like phenotypes in experimental rodents.[36,37] The apparatus used was an elevated four-arm maze having two open (unprotected) and two enclosed (protected) arms converging on a central square. Reduced preference for open arms of the EPM is regarded as an index of anxiety-like states, and clinically-effective drugs with anxiolytic activity have been consistently demonstrated to increase the time that rodents spend in the open arms.[36,37]
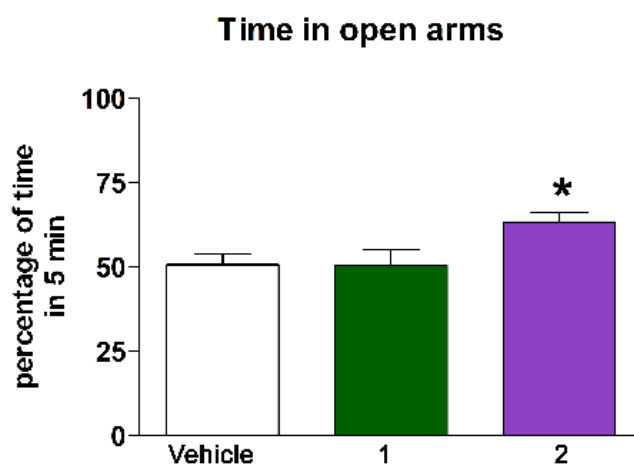
Figure 5. Effects of the acute administration of **1** (30 mg/kg, i.p.) and **2** (30 mg/kg, i.p.) on the percentage of time spent by rats in the open arms of the EPM. *$p < 0.05$ as compared with vehicle-treated rats, N = 7 for each experimental group.

Acute administration of **2** (30 mg/kg, i.p.) significantly increased the percentage of time that rats spent in the open arms (t=2.79, df=12, p=0.03, Figure 5), compared with vehicle. Conversely, acute administration of **1** (30 mg/kg, i.p.) had no effects on rats' preference for open arms (t=0.69, df=12, p=0.47, Figure 5), compared with the vehicle. In addition, acute administration of **2** (30 mg/kg, i.p.) significantly reduced the percentage of time that rats spent in the closed arms, compared with vehicle, while acute administration of **1** (30 mg/kg, i.p.) did not produce the same effect (data not shown). Based on these

15

results, it can be concluded that the ability to induce anxiolytic-like effects observed for the two PIGA compounds correlates with their steroidogenic efficacies, which in turn positively correlated with their RTs to TSPO. These results strongly support the hypothesis that the observed pharmacological effect is due to the specific interaction of PIGAs with TSPO, excluding any other off-target effect.

All in all, the data from this study give a viable model for the rational design of TSPO ligands with therapeutic potential in humans for pathological conditions that will benefit from an enhanced neurosteroidogenesis. Actually, the positive correlation among increased RT, enhanced steroid production and biological in vivo effects, herein rationalized by means of computational methods, has been reported not only for several PIGA compounds[17,18] (see Table 1 and Table S1 in SI), but also for the reference ligands **3**[17](see Table 1) and Ro5-4864,[38] as well as the clinically active anxiolytics XBD173 (emapunil)[39] and etifoxine.[38] Furthermore, many literature reports demonstrated that data achieved employing rTSPO as a working model can be translatable to human TSPO studies. In particular, these data were already useful to develop both pharmacologically effective compounds [40,41] and biomarkers for positron emission tomography (PET) imaging of TSPO in the human brain,[42,43] including a ^{11}C-radioligand featuring the PIGA chemotype.[44] Moreover, the activity of TSPO compounds in clinical trial or already employed in the clinical practice such as XBD173 and etifoxine, respectively, were also confirmed in rodents, further substantiating the transferrability of the in silico, in vitro and in vivo results achieved on rTSPO in humans.

Conclusions

TSPO is a validated pharmacological target for CNS diseases. PIGA compounds have been widely characterized as TSPO ligands as well as for their therapeutic potential. It is now clear that the main key parameter to consider in the discovery of biologically efficacious PIGAs is the RT at TSPO rather than

their affinity for the target. Starting from these data, here we unraveled the structural reasons for different RTs of PIGAs with a similarly high affinity at TSPO by setting up an enhanced-sampling MD protocol. In particular, we studied the unbinding of two PIGAs by RAMD and SMD simulations. Results of this inspection outlined how a slow-unbinding PIGA is able to establish, during its egress, tight interactions at the interface between LP1, TM2, and TM5 TSPO regions. On the other hand, a biologically inefficacious and fast-unbinding PIGA is unable to establish stable interactions with this protein area.

While laying the basis for the rational design of new TSPO agents endowed with high biological efficacy, our studies also add another piece to the puzzle of the so far elusive TSPO activation mechanism. In particular, our studies give a viable model to explain how slow-unbinding PIGAs are able to effectively influence the recognition of cholesterol by TSPO as well as its monomeric/dimeric state. Stimulated by the present work, future structural studies will further support such a hypothesis.

Methods.

General Chemistry Directions.

1[3] and **2**[5] were prepared in two steps, as previously described. Briefly, acylation of the 2-aryl-indoles with oxalyl chloride furnished the corresponding 2-arylindolylglyoxylyl chlorides, which, through subsequent reaction with the appropriate dialkylamine, yield the target compounds;[3,5] the first step was conducted at room temperature in anhydrous diethyl ether, the second one in dry toluene solution, at room temperature and in the presence of triethylamine.[3,5]

Biological evaluation: thermodynamic, kinetic parameters and neurosteroidogenic efficacy

PIGA ligands' binding parameters at the [³H]PK11195 binding site were assessed as previously described.[17] In particular, the K_i and RT values were determined by "displacement competition" and "competition kinetic association" assay, respectively. The ligand ability to stimulate neurosteroidogenis was investigated in an in vitro well-validated neurosteroidogenic C6 rat glioma cell model, as previously reported.[17,39] Briefly, in conditioned serum-free medium derived by the PIGA-treated cells, the amount of the first product of neurosteroidogenesis pregnenolone was measured blocking its further metabolism by trilostane and SU10603. PIGA ligand efficacy (Emax value, relative to the highest tested concentration of TSPO ligand) was calculated with respect to the basal pregnenolone production (sample treated with DMSO).[17]

Molecular Modeling Methods: Docking.

The previously developed rTSPO model,[5] generated using as a template the reported mouse solution structure of TSPO (PDB code 2MGY),[24] was employed for docking experiments attained on compounds **1**, **2,** and **3**. Docking studies were attained using Glide within Maestro9.8.[45] The 3D structures of **1** and **2** were obtained with the Maestro fragment Build tool and then geometrically and energetically optimized with Macromodel.[45] Then, the rTSPO structure was prepared with the protein preparation wizard of Maestro 9.8,[45] which correctly ascribes bond orders, adds hydrogens, and generates proper protomeric states. The grid box for docking calculations was centered on the residues of the binding pocket of **3**, with a grid box of 24 Å × 24 Å × 24 Å. The residues considered belonging to the binding sites used for the grid center calculations are A23, V26, L49, A50, I52, W107, V110, L114, A147, and L150. Docking calculations were all attained using the standard precision (SP) mode.

Molecular Modeling Methods: Molecular Dynamics simulations.

System Preparation. The rTSPO-ligand complexes, thus obtained, were parameterized using *ff14SB* and *gaff* as force fields.[46] The N-terminal and the C-terminal amino acids were capped with ACE and NME, respectively. The systems were embedded into an explicit POPC:cholesterol bilayer (2:1 ratio), as previously described,[47,48] and TIP3P was used as water model.

Molecular Dynamics simulations. MD simulations were attained with NAMD2.8.[49] The prepared systems were progressively minimized and subsequently equilibrated for 5 ns. In every equilibration step, the NPT ensemble was employed with a pressure target of 1 atm, and temperature equal to 300 K. The cutoff of nonbonded interactions was of 10 Å, and the PME algorithm was employed with a grid spacing of 1 Å. We attained a two-steps equilibration approach. Each of these steps lasted for 2.5 ns, using an integration step of 1 fs. The first 2.5 ns of the equilibration step was run by adding harmonic constraints of 2 kcal/mol*Å^{-2} to the protein backbone atoms as well as on all the atoms of the ligand. For the remaining 2.5 ns, the identical MD settings were used and the positional constraints on the aforementioned atoms were scaled down to 1 kcal/mol*Å^{-2}. Lastly, a 50 ns production calculation was attained for each studied system. Of these 50 ns, 25 ns were attained employing the NPT ensemble, whereas the NVT ensemble was selected for the remaining 25 ns, to prepare the studied systems for the subsequent RAMD and SMD calculations. In the production step, we selected an integration step of 2 fs applying constrains on all bonds involving hydrogen atoms.

RAMD and Ligand Unbinding Reaction Coordinates. Recently RAMD has been effectively employed to reveal presumed ligand unbinding pathways for pertinent pharmacological targets.[25,26,50,51] In RAMD calculations, a randomly oriented force (*f*) is imposed to the center of mass of a set of atoms, in our case those belonging to the ligand, for a well-defined short extent of time-steps (*N*). Today, RAMD can be attained employing two different approaches: (*i*) pure RAMD calculations where the randomly-oriented acceleration is continuously imposed, and (ii) combined RAMD-MD simulations where RAMD and MD

steps are alternated. For the rTSPO-ligand complexes, the second approach (RAMD-MD) was employed. The initial conformation was represented by the complex obtained after the 25 ns of standard MD simulations using the NVT ensemble, the constant force was imposed to all the heavy atoms belonging to the ligand and 10 independent RAMD calculations were run for every complex. The unbinding pathway of each ligand was profiled using VMD1.9.2[52] by tracking the center of mass calculated considering the heavy atoms of the ligand. For each rTSPO-ligand complex, the most probable unbinding pathway was then selected as a reaction coordinate for the unbinding event and subsequently used to reconstruct the profile of the free-energy for the unbinding of each ligand and for the subsequent SMD simulations.

Steered Molecular Dynamics (SMD) simulations and PMF calculations. Every the SMD calculations were attained employing the NVT ensemble and using NAMD2.8 and plumed 1.3.[53] PMF along the unbinding reaction coordinate was rebuilt from unidirectional constant-velocity pulling trajectories of the SMD, so as to pull the ligand center of mass far away 30 Å from the center of mass of the binding site. Ten independent 20 ns long SMD trajectories were calculated for each system, for a total time of 600 ns of SMD simulation. Every SMD run was obtained applying a pulling velocity (v) of 0.003 Å/ps. The value of the imposed force (f) was saved every 2 ps (dt), and the work employed on the studied system during SMD was obtained by numerical integration (eq. 1). The stiff spring approximation (eq. 2)[23] was fulfilled with a spring constant (KAPPA in plumed 1.3) of 500 kJ/mol (119,503 kcal/mol). This specific value was selected by employing the following optimization step, previously reported:[27] (i) Initial SMD simulations were calculated on the rTSPO-**1** (fast dissociating ligand) and rTSPO-**2** (slow dissociating ligand) complexes by selecting the spring constant value to 10, 100, 250, 500, and 1000 kJ/mol. (ii) Spring constant values were set to allow for the preservation of the stiff spring approximation for the studied systems and definition of the spring value range (500−1000 kJ/mol) to be evenly explored (100 kJ/mol) with additional SMD runs with both systems. (iii) The smallest spring constant value that allows for the preservation of the stiff spring approximation in both systems (500 kJ/mol) was chosen. PMF along the

unbinding reaction coordinate was rebuilt from the trajectories obtained from the above described SMD calculations and employing Jarzynski's equality (eq. 3).[23,54,55] The cumulant expansion approach up to second order (eq. 4)[20] was used to rebuild the PMF.

$$W_{[x_{(t)}]} = \int_0^{x_{(t)}} F_{(t)} dx_{(t)} \qquad \text{eq. 1}$$

$$F_{(\lambda)} \cong \phi_\lambda \qquad \text{eq. 2}$$

$$e^{-\beta \Delta F} = \langle e^{-\beta W} \rangle \qquad \text{eq. 3}$$

$$\Delta F = \langle W \rangle - \frac{\sigma^2 W}{2 k_B T} \qquad \text{eq. 4}$$

where $\sigma^2 W = \langle W^2 \rangle - \langle W \rangle^2$ and $k_B T = 0{,}598637056$

Cluster analysis. For every studied system all the SMD trajectories were concatenated and clustering of the different conformations was attained employing the AmberTool16 *ptraj* tool.[46] All the trajectories were aligned on the initial frame used as starting point of the SMD simulations and clustered according to the root mean square deviation (r.m.s.d.) of the ligand atoms and the Cα atoms of P41 and T149. The average linkage cluster analysis algorithm was employed, the cutoff distance was set to 1 Å, while the most representative structure (namely the SMD frame closest to the centroid of each cluster) was employed and analyzed to obtain structural information. All pictures were rendered using the UCSF Chimera software.

In vivo pharmacological evaluation of PIGA ligands.

In vivo experiments were performed in male Sprague—Dawley rats (N = 21; Harlan, Italy) weighing 180—200 g. Animals were kept in groups of 4-5 per cage in a room at a temperature of 24 °C and under a 12 h light/dark cycle (lights on at 08:00 h). Food and water were available *ad libitum*, except during behavioral evaluation of EPM performance. Experiments were conducted according to the European Communities Directive for the care and use of experimental animals (86/609/EEC; D.L., 27.01.1992, number 116) and with the guidelines approved by the Ethical Committee of Cagliari University.

PIGA ligands were administered to rats 30 min before behavioral evaluation by the intraperitoneal route (1 ml/100 g of body weight) in a suspension prepared using 0.5% methylcellulose + 0.5% DMSO + 1% Tween-80 in distilled water (VEH). VEH alone was administered to control animals. PIGA ligands were administered at the dose of 30 mg/kg, selected according to previous results of our group showing that rats display increased preference for open arms in the EPM when treated with the same dose of TSPO ligands structurally similar to those investigated here.[4,16]

Evaluation of rats' performance in the EPM was performed basically according to Costa et al.[16] The apparatus was made of white PVC and had two opposite open arms and two opposite closed arms (for each arm: length 50 cm; width10 cm); closed arms had walls (height: 40 cm) along their length. The arms of the EPM converged on a central square (10 cm × 10 cm), and the maze was elevated 50 cm from the floor. Rats used in the present study were naïve to the EPM and were individually tested. Testing was performed by individually placing rats in the central square with the snout directed towards an open arm and leaving them free to explore the EPM for 5 min. The behavioral evaluation was conducted under the illumination of 40 lux, and the surface of the EPM was subjected to uniform illumination. Behavior in the EPM was videotaped for each rat, and later evaluated in order to score the percentage of time spent in open and closed arms, based on the total number of seconds each rat spent in the four arms. Rats were considered to be inside an arm when they had all the four paws inside it.

Statistical analysis. Means ± SEM of the percentages of time spent in open arms of the EPM were calculated. Unpaired *t*-test was used to evaluate differences in open arm preference between rats treated with either PIGA ligand and rats treated with vehicle. The Graph-Pad Prism 4 software (Graph-Pad Software Inc, San Diego, CA) was used to perform statistical analysis.

Associated Content

Supporting Information. Additional table. Videos of the simulated unbinding of **1** and **2**. PDB files of the calculated complexes. This material is available free of charge via the Internet at http://pubs.acs.org.

Author Information

Corresponding Author

* To whom all correspondence should be addressed. S. Cosconati, Tel: +39 0823274789. Fax: +39 0823274585. E-mail: sandro.cosconati@unicampania.it; S. Taliani, Tel: +39 0502219547. Fax: +39 0502219605; E-mail: sabrina.taliani@unipi.it.

Author Contributions

The manuscript was written through the contributions of all authors.

Abbreviations

PIGAs, *N,N*-dialkyl-2-phenylindol-3-ylglyoxylamides; TSPO translocator protein 18 kDa; RT, residence time; GABA$_A$R, γ-aminobutyric acid type A receptor; EPM, elevated plus-maze; SKR, structure−kinetic relationship; MD, molecular dynamics; SMD, steered molecular dynamics; RAMD, random acceleration molecular dynamics; PMF, potential of mean force.

References

1. Copeland, R. A. The drug-target residence time model: a 10-year retrospective. *Nat. Rev. Drug. Discov.* **2016**, *15*, 87–95.

2. Schuetz, D. A.; de Witte, W. E. A.; Wong, Y. C.; Knasmueller, B.; Richter, L.; Kokh, D. B.; Sadiq, S. K.; Bosma, R.; Nederpelt, I.; Heitman, L. H.; Segala, E.; Amaral, M.; Guo, D.; Andres, D.; Georgi, V.; Stoddart, L. A.; Hill, S.; Cooke, R. M.; De Graaf, C.; Leurs, R.; Frech, M.; Wade, R. C.; de Lange, E. C. M.; AP, I. J.; Muller-Fahrnow, A.; Ecker, G. F. Kinetics for Drug Discovery: an industry-driven effort to target drug residence time. *Drug. Discov. Today* **2017**, *22*, 896–911.

3. Primofiore, G.; Da Settimo, F.; Taliani, S.; Simorini, F.; Patrizi, M. P.; Novellino, E.; Greco, G.; Abignente, E.; Costa, B.; Chelli, B.; Martini, C. *N,N*-dialkyl-2-phenylindol-3-ylglyoxylamides. A new class of potent and selective ligands at the peripheral benzodiazepine receptor. *J. Med. Chem.* **2004**, *47*, 1852–1855.

4. Da Settimo, F.; Simorini, F.; Taliani, S.; La Motta, C.; Marini, A. M.; Salerno, S.; Bellandi, M.; Novellino, E.; Greco, G.; Cosimelli, B.; Da Pozzo, E.; Costa, B.; Simola, N.; Morelli, M.; Martini,

C. Anxiolytic-like effects of *N,N*-dialkyl-2-phenylindol-3-ylglyoxylamides by modulation of translocator protein promoting neurosteroid biosynthesis. *J. Med. Chem.* **2008**, *51*, 5798–5806.

5. Barresi, E.; Bruno, A.; Taliani, S.; Cosconati, S.; Da Pozzo, E.; Salerno, S.; Simorini, F.; Daniele, S.; Giacomelli, C.; Marini, A. M.; La Motta, C.; Marinelli, L.; Cosimelli, B.; Novellino, E.; Greco, G.; Da Settimo, F.; Martini, C. Deepening the topology of the Translocator Protein binding site by novel *N,N*-dialkyl-2-arylindol-3-ylglyoxylamides. *J. Med. Chem.* **2015**, *58*, 6081–6092.

6. Papadopoulos, V.; Baraldi, M.; Guilarte, T. R.; Knudsen, T. B.; Lacapere, J. J.; Lindemann, P.; Norenberg, M. D.; Nutt, D.; Weizman, A.; Zhang, M. R.; Gavish, M. Translocator protein (18kDa): new nomenclature for the peripheral-type benzodiazepine receptor based on its structure and molecular function. *Trends Pharmacol Sci* **2006,** *27*, 402-409.

7. Midzak, A.; Zirkin, B.; Papadopoulos, V. Translocator protein: pharmacology and steroidogenesis. *Biochem. Soc. Trans.* **2015**, *43*, 572–578.

8. Reddy, D. S. Neurosteroids: endogenous role in the human brain and therapeutic potentials. *Prog. Brain. Res.* **2010**, *186*, 113–137.

9. Taliani, S.; Da Settimo, F.; Da Pozzo, E.; Chelli, B.; Martini, C. Translocator protein ligands as promising therapeutic tools for anxiety disorders. *Curr. Med. Chem.* **2009**, *16*, 3359-3380.

10. Taliani, S.; Pugliesi, I.; Da Settimo, F. Structural requirements to obtain highly potent and selective 18 kDa Translocator Protein (TSPO) ligands. *Curr. Top. Med. Chem*. **2011**, *11*, 860–886.

11. Simorini, F.; Marini, A. M.; Taliani, S.; La Motta, C.; Salerno, S.; Pugliesi, I.; Da Settimo, F. Medicinal chemistry of indolylglyoxylamide TSPO high affinity ligands with anxiolytic-like effects. *Curr Top Med Chem.* **2012**, *12*, 333-351.

12. Da Pozzo, E.; Giacomelli, C.; Barresi, E.; Costa, B.; Taliani, S.; Passetti Fda, S.; Martini, C. Targeting the 18-kDa translocator protein: recent perspectives for neuroprotection. *Biochem. Soc. Trans.* **2015**, *43*, 559–565.

13. Kim, T.; Pae, A. N. Translocator protein (TSPO) ligands for the diagnosis or treatment of neurodegenerative diseases: a patent review (2010-2015). *Expert Opin. Ther. Pat.* **2016,** *26*, 1325-1351.

14. Santoro, A.; Mattace Raso, G.; Taliani, S.; Da Pozzo, E.; Simorini, F.; Costa, B.; Martini, C.; Laneri, S.; Sacchi, A.; Cosimelli, B.; Calignano, A.; Da Settimo, F.; Meli, R. TSPO-ligands prevent oxidative damage and inflammatory response in C6 glioma cells by neurosteroid synthesis. *Eur. J. Pharm. Sci.* **2016**, *88*, 124–131.

15. Da Pozzo, E.; Giacomelli, C.; Costa, B.; Cavallini, C.; Taliani, S.; Barresi, E.; Da Settimo, F.; Martini, C. TSPO PIGA ligands promote neurosteroidogenesis and human astrocyte well-being. *Int. J. Mol. Sci.* **2016**, *17*, E1028.

16. Costa, B.; Da Pozzo, E.; Chelli, B.; Simola, N.; Morelli, M.; Luisi, M.; Maccheroni, M.; Taliani, S.; Simorini, F.; Da Settimo, F.; Martini, C. Anxiolytic properties of a 2-phenylindolglyoxylamide TSPO ligand: Stimulation of in vitro neurosteroid production affecting GABAA receptor activity. *Psychoneuroendocrinology* **2011**, *36*, 463–472.

17. Costa, B.; Da Pozzo, E.; Giacomelli, C.; Barresi, E.; Taliani, S.; Da Settimo, F.; Martini, C. TSPO ligand residence time: a new parameter to predict compound neurosteroidogenic efficacy. *Sci. Rep.* **2016**, *6*, 18164.

18. Costa, B.; Taliani, S.; Da Pozzo, E.; Barresi, E.; Robello, M.; Cavallini, C.; Cosconati, S.; Da Settimo, F.; Novellino, E.; Martini, C. Residence time, a new parameter to predict neurosteroidogenic efficacy of Translocator Protein (TSPO) ligands: the case study of *N,N*-dialkyl-2-arylindol-3-ylglyoxylamides. *ChemMedChem* **2017**, *12*, 1275–1278.

19. Scarf, A. M.; Auman, K. M.; Kassiou, M. Is there any correlation between binding and functional effects at the translocator protein (TSPO) (18 kDa)? *Curr. Mol. Med.* **2012**, *12*, 387–397.

20. Isralewitz, B.; Gao, M.; Schulten, K. Steered molecular dynamics and mechanical functions of proteins. *Curr. Opin. Struct. Biol.* **2001**, *11*, 224–230.

21. Hamelberg, D.; Mongan, J.; McCammon, J. A. Accelerated molecular dynamics: a promising and efficient simulation method for biomolecules. *J. Chem. Phys.* **2004**, *120*, 11919–11929.

22. Tiwary, P.; Salvalaglio, V.L.M.; Parrinello, M. Kinetics of protein–ligand unbinding: Predicting pathways, rates, and rate-limiting steps. *Proc. Natl. Acad. Sci. U. S. A.* **2015**, *112*, E386-E391.

23. Jarzynski, C. Nonequilibrium Equality for Free Energy Differences. *Phys. Rev. Lett.* **1997**, *78*, 2690-2693.

24. Jaremko, Ł.; Jaremko, M.; Giller, K.; Becker, S.; Zweckstetter, M. Structure of the mitochondrial translocator protein in complex with a diagnostic ligand. *Science* **2014**, *343*, 1363–1366.

25. Carlsson, P.; Burendahl, S.; Nilsson, L. Unbinding of retinoic acid from the retinoic acid receptor by random expulsion molecular dynamics. *Biophys. J.* **2006**, *91*, 3151–3161.

26. Colizzi, F.; Perozzo, R.; Scapozza, L.; Recanatini, M.; Cavalli, A. Single-molecule pulling simulations can discern active from inactive enzyme inhibitors. *J. Am. Chem. Soc.* **2010**, *132*, 7361–7371.

27. Capelli, A. M.; Bruno, A.; Entrena Guadix, A.; Costantino, G. Unbinding pathways from the glucocorticoid receptor shed light on the reduced sensitivity of glucocorticoid ligands to a naturally occurring, clinically relevant mutant receptor. *J. Med. Chem.* **2013**, *56*, 7003–7014.

28. Liphardt, J.; Dumont, S.; Smith, S. B.; Tinoco, I. Jr.; Bustamante, C. Equilibrium information from nonequilibrium measurements in an experimental test of Jarzynski's equality. *Science* **2002**, *296*, 1832–1835.

29. Martinez-Rosell, G.; Giorgino, T.; Harvey, M. J.; de Fabritiis, G. Drug discovery and molecular dynamics: methods, applications and perspective beyond the second timescale. *Curr. Top. Med. Chem.* **2017**, *17*, 2617–2625.

30. De Vivo, M.; Masetti, M.; Bottegoni, G.; Cavalli, A. Role of molecular dynamics and related methods in drug discovery. *J. Med. Chem.* **2016**, *59*, 4035–4061.

31. Schmidtke, P.; Luque, F. J.; Murray, J. B.; Barril, X. Shielded hydrogen bonds as structural determinants of binding kinetics: application in drug design. *J. Am. Chem. Soc.* **2011**, *133*, 18903–18910.

32. Li, H.; Papadopoulos, V. Peripheral-type benzodiazepine receptor function in cholesterol transport. Identification of a putative cholesterol recognition/interaction amino acid sequence and consensus pattern. *Endocrinology.* **1998**, *139*, 4991–4997.

33. Farges, R.; Joseph-Liauzun, E.; Shire, D.; Caput, D.; Le Fur, G.; Ferrara, P. Site-directed mutagenesis of the peripheral benzodiazepine receptor: identification of amino acids implicated in the binding site of Ro5-4864. *Mol. Pharmacol.* **1994**, *46*, 1160–1167.

34. Li, F.; Liu, J.; Liu, N.; Kuhn, L. A.; Garavito, R. M.; Ferguson-Miller, S. Translocator Protein 18 kDa (TSPO): an old protein with new functions? *Biochemistry.* **2016**, *55*, 2821–2831.

35. Jaipuria, G.; Leonov, A.; Giller, K.; Vasa, S.K.; Jaremko, Ł.; Jaremko, M.; Linser R, Becker S, Zweckstetter M. Cholesterol-mediated allosteric regulation of the mitochondrial translocator protein structure. *Nat. Commun*. **2017,** *8*, 14893.

36. Pellow, S.; Chopin, P.; File, S. E.; Briley, M. Validation of open:closed arm entries in an elevated plus-maze as a measure of anxiety in the rat. *J. Neurosci. Methods* **1985**, *14*, 149-167.

37. Dawson, G. R.; Tricklebank, M. D. Use of the elevated plus maze in the search for novel anxiolytic agents. *Trends Pharmacol. Sci.* **1995**, *16*, 33-36.

38. Costa, B.; Cavallini, C.; Da Pozzo, E.; Taliani, S.; Da Settimo, F.; Martini, C. The anxiolytic etifoxine binds to TSPO Ro5-4864 binding site with long residence time showing a high neurosteroidogenic activity. *ACS Chem. Neurosci.* **2017**, *8*, 1448-1454.

39. Costa, B.; Da Pozzo, E.; Cavallini, C.; Taliani, S.; Da Settimo, F.; Martini, C. Long Residence Time at the neurosteroidogenic 18 kDa Translocator Protein characterizes the anxiolytic ligand XBD173. *ACS Chem. Neurosci.* **2016**, *7*, 1041–1046.

40. Kita, A.; Kinoshita, T.; Kohayakawa, H.; Furukawa, K.; Akaike, A. Lack of tolerance to anxiolysis and withdrawal symptoms in mice repeatedly treated with AC-5216, a selective TSPO ligand. *Prog. Neuro-Psychopharmacol. Biol. Psychiatry* **2009**, *33*, 1040−1045.

41. Rupprecht, R.; Rammes, G.; Eser, D.; Baghai, T. C.; Schule, C.; Nothdurfter, C.; Troxler, T.; Gentsch, C.; Kalkman, H. O.; Chaperon, F.; Uzunov, V.; McAllister, K. H.; Bertaina-Anglade, V.; La Rochelle, C. D.; Tuerck, D.; Floesser, A.; Kiese, B.; Schumacher, M.; Landgraf, R.; Holsboer, F.; Kucher, K. Translocator protein (18 kDa) as target for anxiolytics without benzodiazepine-like side effects. *Science* **2009**, *325*, 490–493.

42. Frankle, W. G.; Narendran, R.; Wood, A. T.; Suto, F.; Himes, M. L.; Kobayashi, M.; Ohno, T.; Yamauchi, A.; Mitsui, K.; Duffy, K.; Bruce, M. Brain translocator protein occupancy by ONO-2952 in healthy adults: a phase 1 PET study using [11C]PBR28. *Synapse* **2017**, doi: 10.1002/syn.21970.

43. Ikawa, M.; Lohith, T. G.; Shrestha, S.; Telu, S.; Zoghbi, S. S.; Castellano, S.; Taliani, S.; Da Settimo, F.; Fujita, M.; Pike, V. W.; Innis, R. B. 11C-ER176, a radioligand for 18-kDa Translocator Protein, has adequate sensitivity to robustly image all three affinity genotypes in human brain. *J. Nucl. Med.* **201**7, *58*, 320-325..

44. Pike, V. W.; Taliani, S.; Lohith, T. G.; Owen, D. R.; Pugliesi, I.; Da Pozzo, E.; Hong, J.; Zoghbi, S. S.; Gunn, R. N.; Parker, C. A.; Rabiner, E. A.; Fujita, M.; Innis, R. B.; Martini, C.; Da Settimo, F. Evaluation of novel N1-methyl-2-phenylindol-3-ylglyoxylamides as a new chemotype of 18 kDa

translocator protein-selective ligand suitable for the development of positron emission tomography radioligands. *J. Med. Chem.* **2011**, *54*, 366-373.

45. Schrodinger Home Page. https://www.schrodinger.com.

46. Amber Home Page. http://ambermd.org.

47. Bruno, A.; Guadix, A. E.; Costantino, G. Molecular dynamics simulation of the heterodimeric mGluR2/5HT(2A) complex. An atomistic resolution study of a potential new target in psychiatric conditions. *J. Chem. Inf. Model.* **2009**, *49*, 1602-1616.

48. Preti, D.; Baraldi, P. G.; Saponaro, G.; Romagnoli, R.; Aghazadeh Tabrizi, M.; Baraldi, S.; Cosconati, S.; Bruno, A.; Novellino, E.; Vincenzi, F.; Ravani, A.; Borea, P. A.; Varani, K. Design, synthesis, and biological evaluation of novel 2-((2-(4-(substituted)phenylpiperazin-1-yl)ethyl)amino)-5'-*N*-ethylcarboxamidoadenosines as potent and selective agonists of the A_{2A} adenosine receptor. *J. Med. Chem.* **2015**, *58*, 3253-3267.

49. NAMD−Scalable Molecular Dynamics. http://www.ks.uiuc.edu/Research/namd/.

50. Ludemann, S. K.; Lounnas, V.; Wade, R. C. How do substrates enter and products exit the buried active site of cytochrome P450cam? 2. Steered molecular dynamics and adiabatic mapping of substrate pathways. *J. Mol. Biol.* **2000**, *303*, 813-830.

51. (a) Magalhaes, J.; Annunziato, G.; Franko, N.; Pieroni, M.; Campanini, B.; Bruno, A.; Costantino, G. Integration of enhanced sampling methods with saturation transfer difference experiments to identify protein druggable pockets. *J. Chem. Inf. Model.* **2018**, *58*, 710-723. (b) Marinelli, L.; Cosconati, S.; Steinbrecher, T.; Limongelli, V.; Bertamino, A.; Novellino, E.; Case, D. A.
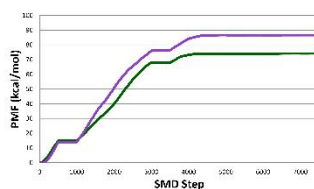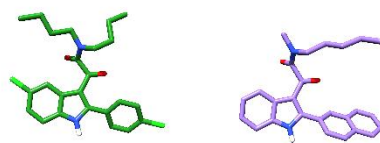
Homology modeling of NR2B modulatory domain of NMDA receptor and analysis of ifenprodil binding. *ChemMedChem.* **2007**, *2*, 1498-1510.

52. VMD−Visual Molecular Dynamics. http://www.ks.uiuc.edu/ Research/vmd/.

53. PLUMED. http://www.plumed.org.

54. Liphardt, J.; Dumont, S.; Smith, S. B.; Tinoco, I. Jr.; Bustamante, C. Equilibrium information from nonequilibrium measurements in an experimental test of Jarzynski's equality. *Science* **2002**, *296*, 1832-1835.

55. Park, S.; Khalili-Araghi, F.; Tajkhorshid, E.; Schulten, K. Free energy calculation from steered molecular dynamics simulations using Jarzynski's equality. *J. Chem. Phys.* **2003**, *119*, 3559-3566.

Table of Contents graphic